SOILS AND FOUNDATIONS Vol. 49, No. 1, 63–74, Feb. 2009
Japanese Geotechnical Society

THE P2S EFFECT ON THE ACCUMULATION OF RESIDUAL STRAINS IN SOFT ROCKS DUE TO IRREGULAR CYCLIC LOADING

D. C. PECKLEY[i] and TARO UCHIMURA[ii]

ABSTRACT

Data and information on the cyclic loading behaviour of soft rocks, especially behaviour under irregular cyclic loading, are very limited. This paper shows that the present procedure of estimating residual strain accumulation due to irregular cyclic loading using a fatigue model from uniform amplitude cyclic loading can result in underestimated residual strains. Such underestimation occurs because the present procedure fails to take into account the so-called P2S effect on the softening behaviour of soft rocks under cyclic loading. The parameter P2S is defined as the sum of the magnitudes of the increments in residual strains due to the previous two loading half-cycles. When P2S is large, a large residual strain increment can be expected. This paper also shows that taking the P2S effect into account can improve the simulation of residual strain accumulation due to irregular cyclic loading.

Key words: irregular cyclic loading, P2S effect, soft rocks, triaxial tests (**IGC**: F7)

INTRODUCTION

The minimal settlements of the piers of the Akashi Kaikyo Bridge, the longest suspension bridge in the world, after the 1995 Kobe Earthquake have demonstrated that soft rocks are competent foundation materials for large-scale structures (Yamagata et al., 1996; Koseki et al., 2001; Kashima et al., 2000). To design more cost-effective, large-scale foundations on soft rocks, however, the deformation characteristics of soft rocks when subjected to large cyclic loading still have to be understood. The forward calculations of the settlements of the piers of the Akashi-Kaikyo Bridge carried out by Koseki et al. (2001) and Kashima et al. (2000) underscored this point. In these calculations, the actual settlements were overestimated by a factor of at least 2.5 times (Koseki et al., 2001) and by as much as 8 times (Kashima et al., 2000). While Koseki et al. (2001) attributed these discrepancies to overestimated seismic accelerations, among other factors, more empirical studies are still needed because of the paucity of data and information regarding cyclic loading behaviour of soft rocks, especially under irregular cyclic loading (Indo, 2001; Salas Monge, 2002; Peckley and Uchimura, 2007).

The fact that heavily populated metropolitan areas such as Tokyo, Japan (Tatsuoka et al., 2003) and Metro Manila, Philippines (Peckley and Uchimura, 2006) are underlain by soft rock formations and are known to be seismically active, is another compelling reason for investigating the strength and deformation characteristics of soft rocks under cyclic loading. In Metro Manila's case, almost 70% of the metropolis is directly underlain by the soft rock formation called the Guadalupe Tuff Formation (GTF). One boundary of this formation is an active fault that can generate an earthquake with a magnitude of 7.2 (Bautista, 2004). A paleoseismic study on the fault that was jointly conducted by the USGS and the Philippine Institute of Volcanology and Seismology or PHIVOLCS (Nelson et al., 2000) indicated a recurrence interval of 200–400 years for magnitude 6–7 earthquakes over the past 1500 years.

In another paper by the same authors (Peckley and Uchimura, 2007), which was submitted to this journal, it was shown that under uniform cyclic loading, longer loading period can result in significantly larger residual strains. In this paper, the behaviour of soft rocks under irregular cyclic loading is examined, starting with a review of the present methodology of estimating residual strain accumulation using a fatigue model from uniform amplitude cyclic loading tests.

TRIAXIAL CYCLIC LOADING TESTS

The soft rock samples, which were tested for this study and are referred herein as GTF samples, were obtained from an excavation into the GTF in Fort Bonifacio, Taguig City, Metro Manila. The excavation was for the basement floors of a multi-story building, which is now under construction. These were extracted by block sampling from a sandstone layer at a depth of around 12 meters from the existing ground elevation. The block samples were then packaged and shipped to the Geo-

[i] Post-doctoral Researcher, Department of Civil Engineering, University of Tokyo, Tokyo, Japan (dan_peckley@yahoo.com).
[ii] Associate Professor, Department of Civil Engineering, University of Tokyo, Tokyo, Japan (uchimura@geot.t.u-tokyo.ac.jp).
The manuscript for this paper was received for review on July 11, 2007; approved on November 27, 2008.
Written discussions on this paper should be submitted before September 1, 2009 to the Japanese Geotechnical Society, 4-38-2, Sengoku, Bunkyo-ku, Tokyo 112-0011, Japan. Upon request the closing date may be extended one month.

technical Engineering Laboratory of the University of Tokyo, Japan, following the recommendations of ASTM D 5079-90 (ASTM, 2000) for critical care to minimize moisture loss and damage in the microstructure of the samples. The samples were cut and trimmed to L100 mm × W60 mm × H150 mm nominal sizes using a rotary cutter. The unit weight of the samples was around 1.78 g/cm^3; moisture content was around 31%; and the mean diameter D_{50} was from 0.20 mm to 0.25 mm (after thorough crushing). The maximum deviator stress q_{max} of the samples at 200 kPa confining pressure and at 1%/min monotonic loading rate was around 3,200 kPa[1].

In the tests, two 120 mm Local Deformation Transducers or LDTs (Goto et al., 1991) were used to measure the longitudinal (axial) deformations and were attached on the 60 mm-wide faces of the specimen. The LDTs were attached to the specimen following the procedure described by Hayano et al. (2001). To measure longitudinal (axial) load, a 50 kN-capacity load cell installed inside the triaxial cell was used to minimize errors due to friction along the loading shaft. Cyclic loading was applied using an oil-hydraulic loading system at the Koseki Laboratory of the Institute of Industrial Science (IIS), University of Tokyo.

Prior to loading, each specimen was consolidated at an isotropic pressure of 200 kPa, the estimated in-situ overburden pressure. The tests were unsaturated because the samples were taken above the water table, which was 20 m below the existing ground surface.

Uniform Amplitude Cyclic Loading Tests

Figure 1 illustrates the loading time-history of the staged cyclic loading tests performed in this study. In the previous uniform amplitude cyclic loading tests that were performed (Peckley and Uchimura, 2006), it was observed that the accumulation of residual strain is almost linear with the number of cycles applied, especially at higher loading amplitudes. Thus, for the tests that were conducted for this study, staged uniform cyclic loading with increasing amplitude for every loading stage was employed. The loading period for all loading stages was at $T = 1$ s. These tests were conducted on samples designated as GTF30, GTF31 and GTF34. Here, only results of the tests on GTF30 and GTF31, shown in Figs. 2 and 3, are included for brevity.

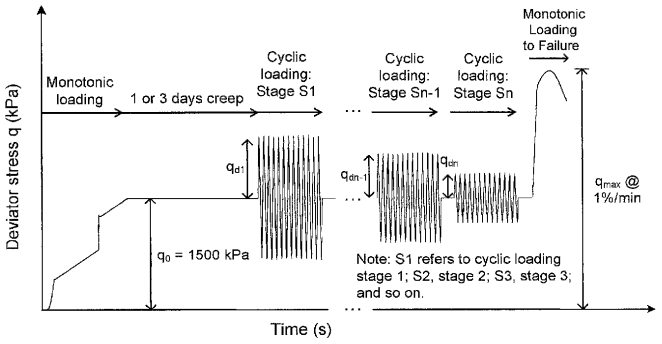

Fig. 1. Staged uniform cyclic loading time-history

Irregular Cyclic Loading Tests

The samples that were subjected to irregular loading

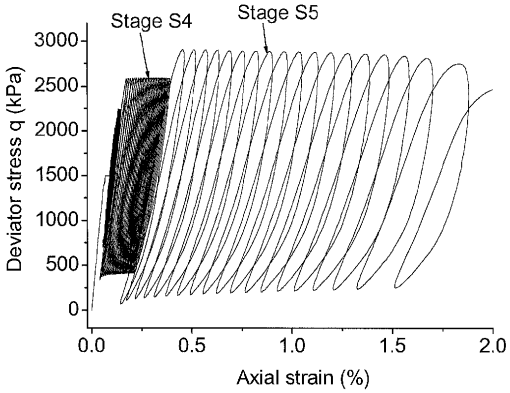

Fig. 2. Cyclic stress-strain curve of GTF30

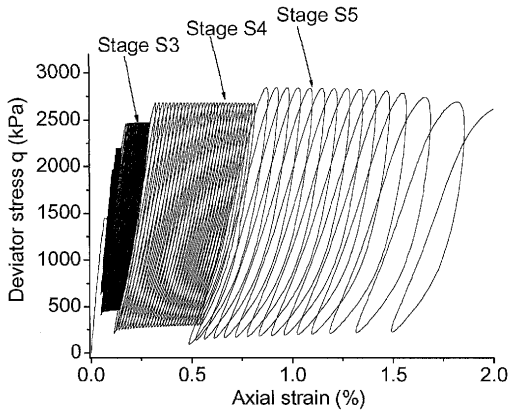

Fig. 3. Cyclic stress-strain curve of GTF34

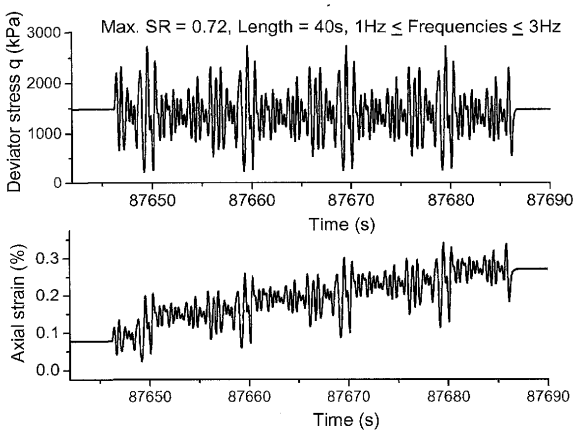

Fig. 4. Stress and strain time histories of GTF33

[1] The tensile strength was not measured. However, since the ratio between the tensile strength and compressive strength of soft rocks can be as high as 0.20 (Coviello et al., 2005), cyclic loading behaviour considering the tensile strength of soft rocks may have to be explored in future studies.

histories were GTF32, GTF33 and GTF35 (Peckley, 2007), but also for brevity only the results of GTF33 and GTF35 are presented. Figures 4 and 5 show the stress-time histories that were applied on these samples and the corresponding strain-time histories that were measured. The cyclic stress-strain curves are shown in Figs. 6 and 7.

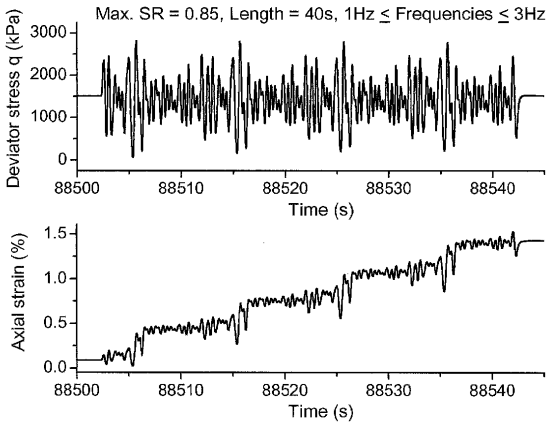

Fig. 5. Stress and strain time histories of GTF35

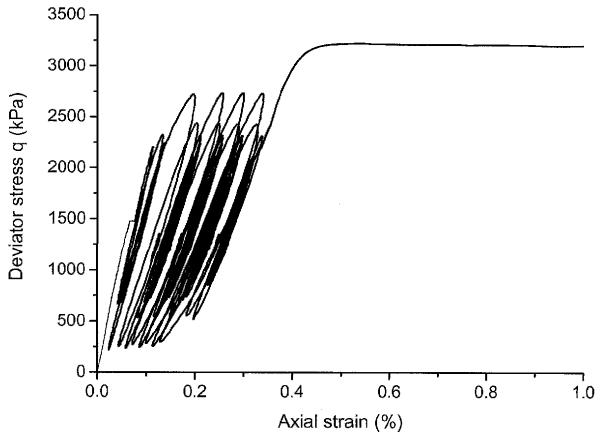

Fig. 6. Cyclic stress-strain curve of GTF33

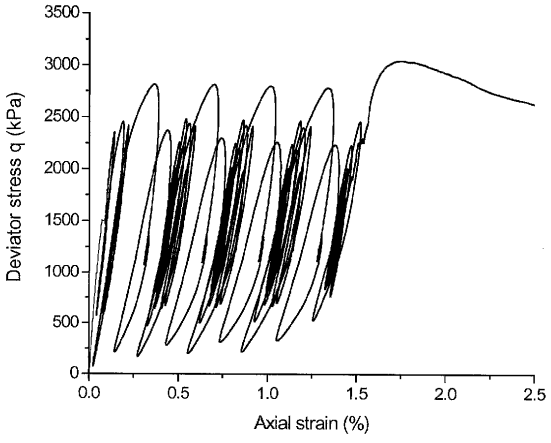

Fig. 7. Cyclic stress-strain curve of GTF35

FATIGUE MODELING AND SIMULATION

The basic assumption employed in fatigue modelling is that the accumulation of residual deformation due to an irregular cyclic loading history can be extrapolated from the evolution of deformations under a series of uniform amplitude cyclic loading tests. The use of fatigue models to evaluate the behaviour of geomaterials due to irregular cyclic loading already has a long history and has been described in detail by a number of prominent researchers, among them, Seed and Idriss (1971), Ishihara and Yasuda (1975), Seed et al. (1975), Tatsuoka and Silver (1981), Tatsuoka et al. (1986), Allotey and El Naggar (2005). Thus, the reader is referred to the works of these researchers for a more detailed treatment on the subject.

Note, however, that in this study the model derived is applicable to loading cases where changes in the direction of the principal axis is not significant and where the tensile strength of the material can be neglected.

Fatigue Model

The results of the uniform amplitude cyclic loading tests (Figs. 2 and 3) can be summarized as shown in Fig. 8, employing the definitions for stress ratio SR, residual strain[2] ε_{ar}, the amplitude of cyclic stress q_d, and the deviator stress at static condition q_0 shown in Fig. 9. The following can be observed from Fig. 8:

a) The accumulation of residual strains is practically linear with the number of cycles applied (CN).
b) The residual strains have an exponential, highly nonlinear relationship with stress ratio SR. Shown also in Fig. 8 is the fatigue model that was obtained by nonlinear curve fitting. Note that in the model the above observations were taken into account.

In the development of the fatigue model, a nonlinear least-squares regression method was employed with the NLSF Advanced Fitting Tool of Origin 7.5 (Originlab

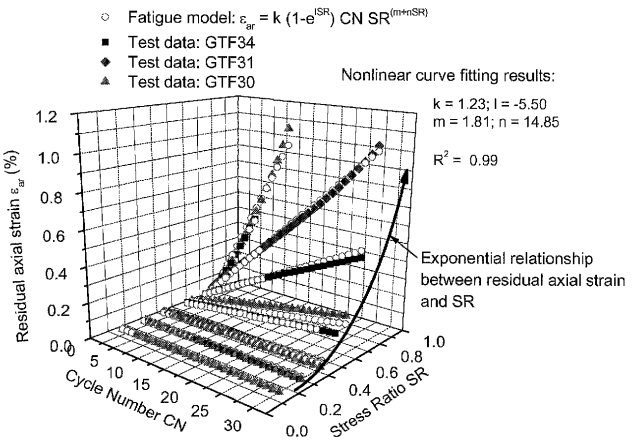

Fig. 8. Comparison between test data and fatigue model (obtained by nonlinear curve fitting)

[2] The residual strain ε_{ar} is measured from the start of the application of cyclic loading, whereas $\Delta\varepsilon_{ar}$ is the increment in residual strain after one cycle, or half cycle. *See Simnlations Using the Fatigue Model.*

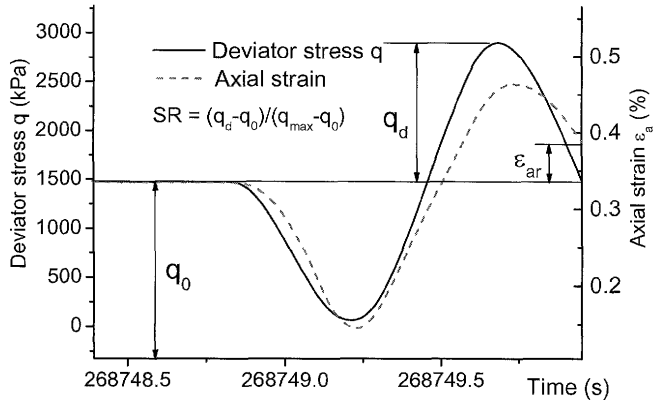

Fig. 9. Definition of Stress Ratio (SR), q_{max} = max. deviator stress (strength) obtained from monotonic loading test

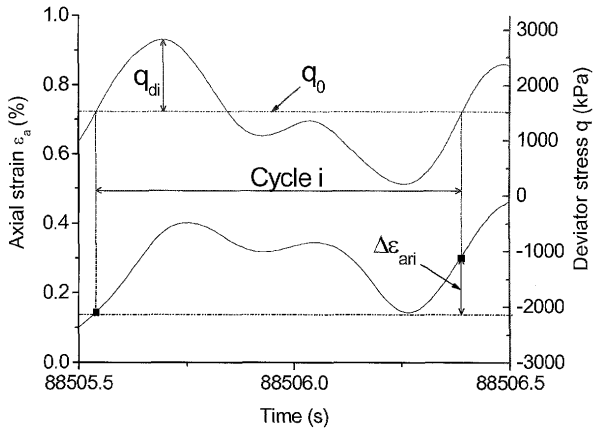

Fig. 10. Definitions of one cycle, cycle i, cycle amplitude q_{di}, and increment in residual strain $\Delta\varepsilon_{ari}$, in irregular cyclic loading

Corporation, 2006). This iterative regression method is based on the Levenberg-Marquardt (LM) algorithm and can simultaneously fit model parameters across data sets. In this case, the fitting parameters were k, l, m and n. The values of these parameters determined after a number of iterations are shown in Fig. 8. In the figure, it can be readily seen that with these parameter values, the model and the test results match with each other well. The coefficient of determination R^2 is 0.99.

It should be noted that with the assumption that strain accumulation is linear with CN, it is implicit that there is one-to-one correspondence between residual strain increment and SR. That is, for every value of SR, there can only be one corresponding value of strain increment.

Simulations Using the Fatigue Model

Consistent with the definitions provided for uniform cyclic loading, the definitions for stress ratio SR and increment in residual strain provided in Fig. 10 are adopted for irregular cyclic loading. As shown, one cycle is defined with the static stress q_0 as reference, irrespective of wave shape. The stress ratio SR for a cycle is determined from the maximum q_d applied in that cycle[3], and residual strain increment is the change in strain after that cycle.

Figures 11 and 12 present the results of the simulations of residual accumulation in samples GTF33 and GTF35 using the fatigue model derived in *Fatique Model*. As shown, the accumulation of residual strains is poorly simulated, especially for GTF35. It can be inferred that as stress ratios become higher, the discrepancies between simulated and measured residual strains become larger.

As the performance at high stress ratio SR values is a primary concern of this study, to account for and explain the discrepancies between measured and simulated residual strains are imperative. As a first step, the measured and simulated residual strains were plotted together with the stress and strain time histories, as shown in Figs. 13 and 14. Taking note that the SR for one cycle of loading is derived from the amplitude of the positive half-cycle, one can observe the following from Figs. 13 and 14:

[3] Note that q_d corresponds to the amplitude of the positive half cycle.

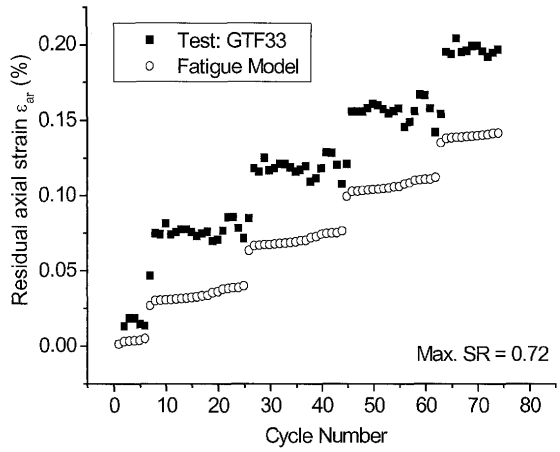

Fig. 11. Accumulated residual strain with cycle number for GTF33

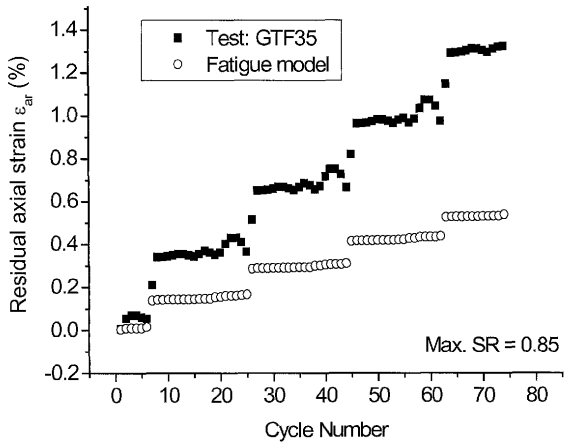

Fig. 12. Accumulated residual strain with cycle number for GTF35

(1) In the case of GTF33 (Fig. 13), it can be observed that while half cycle 'b' has a higher amplitude than half cycle 'c', the maximum strains and residual strain increments due to these half cycles are almost the same. It appears that after half cycle 'b', softening had occurred, resulting in a residual

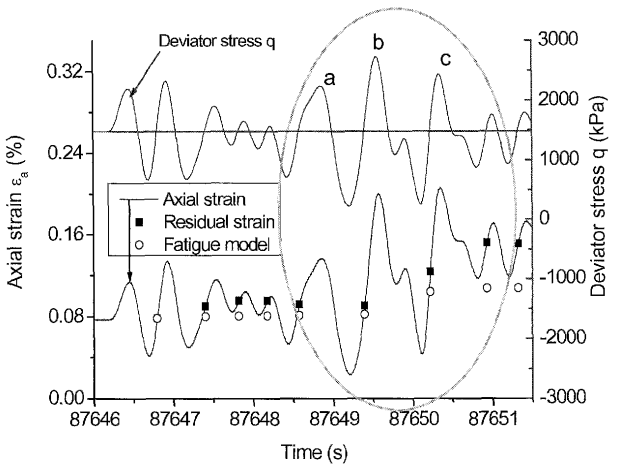

Fig. 13. Accumulated residual strain with time for GTF33

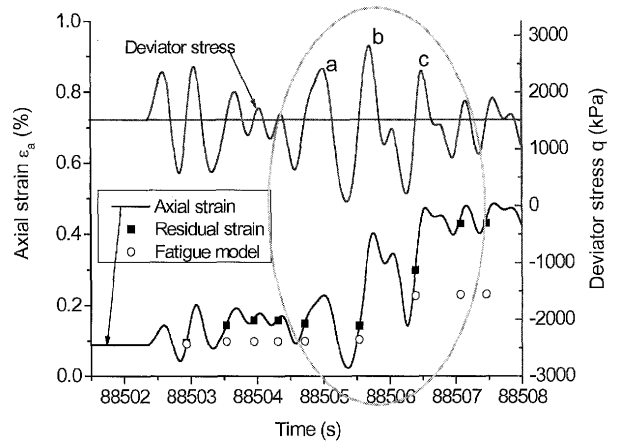

Fig. 14. Accumulated residual strain with time for GTF35

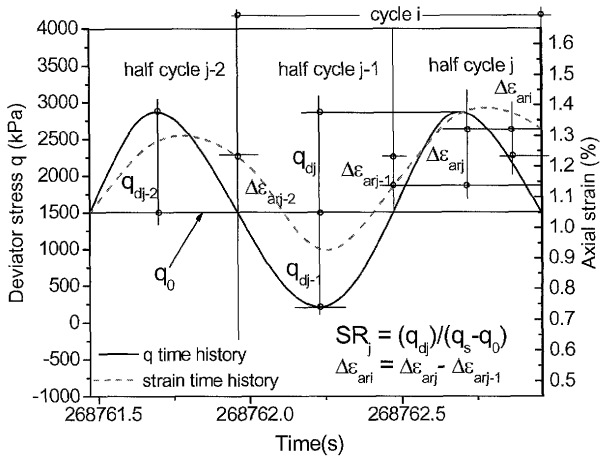

Fig. 15. Definition of half-cycle j and corresponding increment in residual strain $\Delta\varepsilon_{arj}$

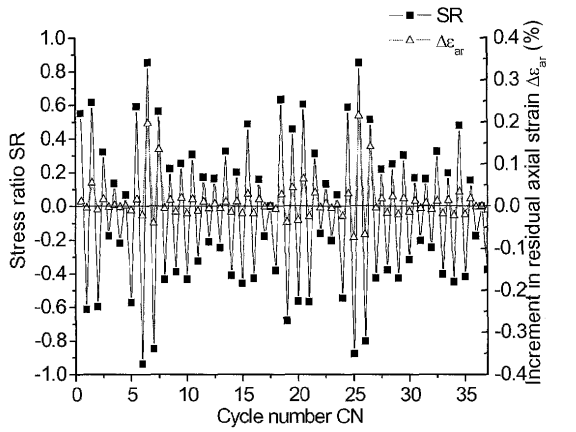

Fig. 16. GTF35 stress ratio SR & increment in residual strain-cycle number history: CN01 to CN37

strain due to half cycle 'c' that was larger than expected.

(2) Similarly, in the case of GTF35 (Fig. 14), it is evident that while half cycles 'a' and 'c' have almost the same amplitudes–and thus, SR values–the residual strain increment due to half cycle 'c' is significantly larger than that of 'a'.

Note that both items completely undermine the validity of the implicit assumption that there is one-to-one correspondence between stress ratio SR (or amplitude) and residual strain increment by virtue of the assumed linear relationship between cycle number CN and residual strain accumulation. Evidently, the fatigue model that was derived cannot be used to simulate residual strain accumulation due to irregular cyclic loading, despite the high value of coefficient of determination R^2 that was obtained. At higher stress ratios, the use of the fatigue model resulted in larger underestimation of residual strains. The apparent reason for this is that it failed to simulate the softening behaviour that occurred after the application of a large load impulse, which were the half cycles indicated as 'b' in Figs. 13 and 14. This softening behaviour is further examined in the following sections.

THE P2S EFFECT

Half-cycle Stress Ratio and Corresponding Increment in Residual Strains

To facilitate the characterization of the behaviour observed in irregular cyclic loadings described above, stress- and strain-time histories are presented in terms of half-cycle stress ratios and their corresponding increment in residual strains, as illustrated in Fig. 15. In this figure, one loading cycle is analyzed in terms of its component positive half-cycle and negative half-cycle. The increment in residual strain is then decomposed also into two components: one corresponds to the positive half-cycle, and the other corresponds to the negative half-cycle. Note that with these definitions, a negative half-cycle results in a negative increment in the residual strain.

When expressed in half-cycle SR and increment in residual strain, the stress and strain time histories (from the start of cyclic loading to $t = 88522$ s) in Fig. 5 become the SR-cycle number (CN) and increment in residual strain-CN histories in Fig. 16.

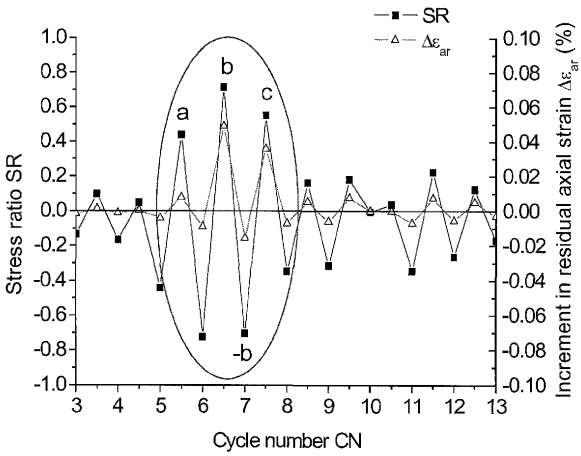

Fig. 17. GTF33 stress ratio SR & increment in residual strain-cycle number history: CN03 to CN13

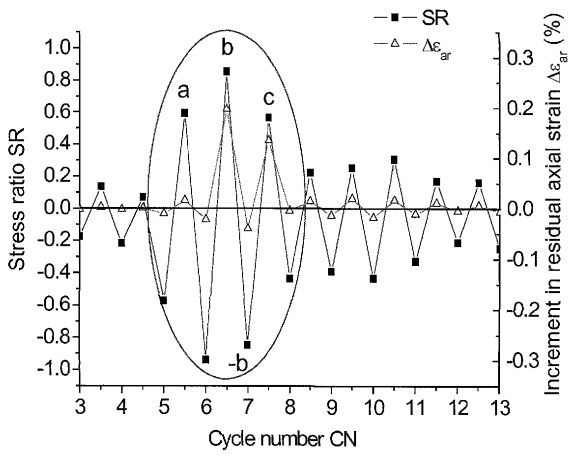

Fig. 19. GTF35 stress ratio SR & increment in residual strain-cycle number history: CN03 to CN13

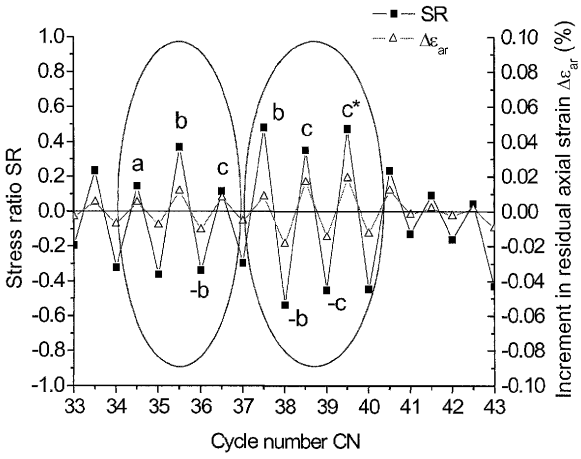

Fig. 18. GTF33 stress ratio SR & increment in residual strain-cycle number history: CN33 to CN43

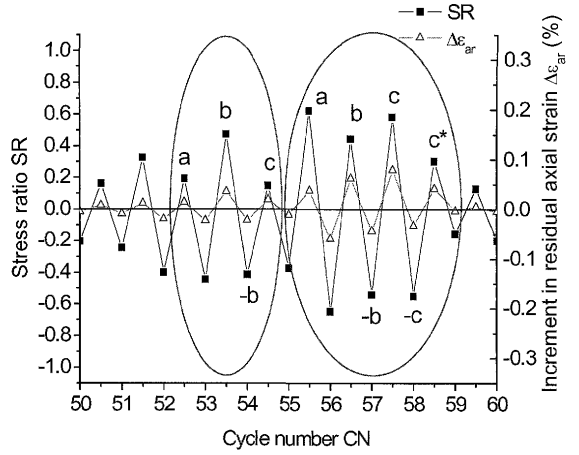

Fig. 20. GTF35 stress ratio SR & increment in residual strain-cycle number history: CN50 to CN60

Relationships between Residual Strain Increment and other Stress-strain Parameters

In the SR-CN and residual strain increment-CN histories of the samples that were subjected to irregular cyclic loading (GTF32, GTF33 and GTF35), a number of segments or windows were selected to further examine the softening behaviour observed in Figs. 12 and 13. These windows include those encircled in Figs. 17 through 20. The basic criteria in selecting these time windows were the following:

1) When there is a deviation from the trend that the higher the stress ratio, the larger the increment in residual strains, as implied in the fatigue model developed in *Fatique Model*.
2) When two half-cycles with essentially the same amplitude have remarkably different increment in residual strain.

The half-cycles where these criteria occurred were then identified and were designated either as 'c' or 'c*', as shown in the figures. To identify the parameter or parameters with which the increment in residual strain is most strongly linked, all the residual strain increments due to these half-cycles were plotted against the current and previous SR parameters, and against the previous residual strain increments.

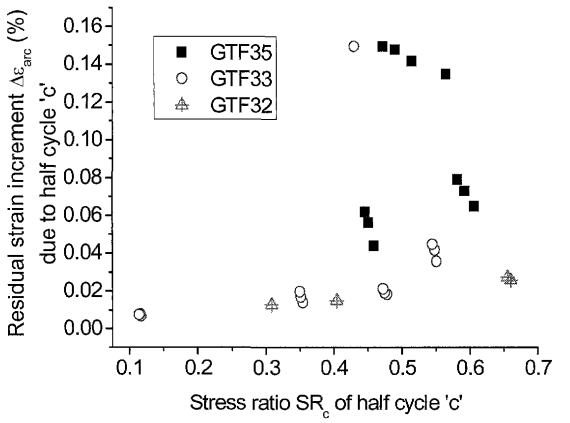

Fig. 21. Increment in residual strain $\Delta\varepsilon_{arc}$ due to half cycle 'c' vs. stress ratio SR_c

Figure 21 plots the increment in residual strain $\Delta\varepsilon_{arc}$ or

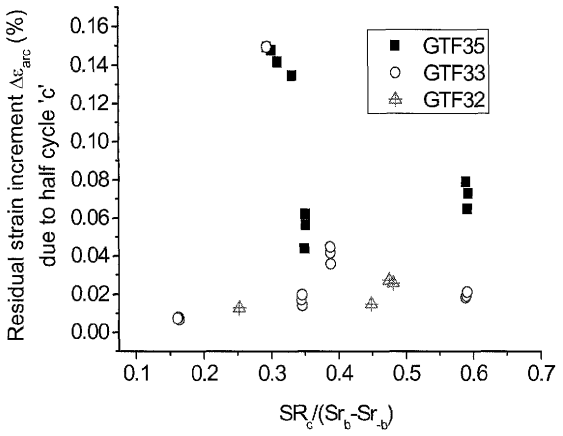

Fig. 22. Increment in residual strain due to half-cycle 'c' $\Delta\varepsilon_{arc}$ vs. the ratio (half cycle SR_c/(half cycle SR_b–half cycle SR_{-b})

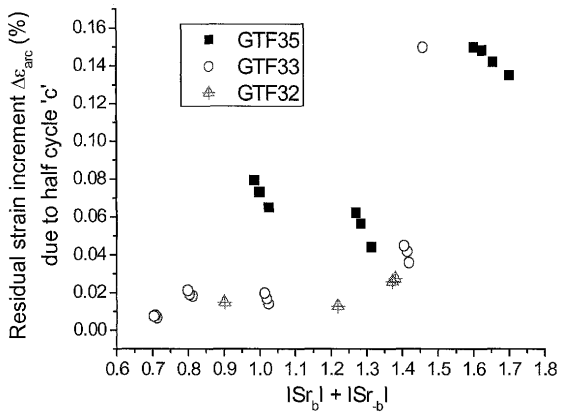

Fig. 23. Increment in residual strain $\Delta\varepsilon_{arc}$ due to half cycle 'c' vs. the sum of the two preceding stress ratios

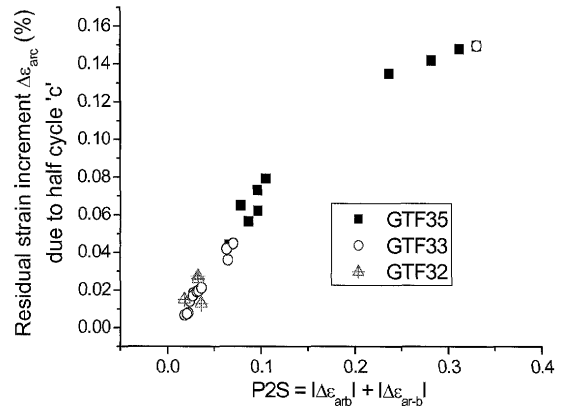

Fig. 24. Increment in residual strain due to half-cycle 'c' $\Delta\varepsilon_{arc}$ vs. P2S = $|\Delta\varepsilon_{arb}| + |\Delta\varepsilon_{ar-b}|$

$\Delta\varepsilon_{arc^*}$ vs. the corresponding stress ratio SR_c or SR_{c^*} and Fig. 22, the increment in residual strain $\Delta\varepsilon_{arc}$ or $\Delta\varepsilon_{arc^*}$ vs. the corresponding ratio $SR_c/(SR_{j-1}\text{-}SR_{-j-2})$. Figure 23 plots the increment in residual strain $\Delta\varepsilon_{arc}$ or $\Delta\varepsilon_{arc^*}$ vs. the sum of the magnitudes of the two preceding stress ratios and Fig. 24, plots $\Delta\varepsilon_{arc}$ or $\Delta\varepsilon_{arc^*}$ vs. the sum of the magnitudes of the increment in residual strain due to the preceding 2 half-cycles ($|\Delta\varepsilon_{arj-1}| + |\Delta\varepsilon_{arj2}|$). Relationships between $\Delta\varepsilon_{arc}$ or $\Delta\varepsilon_{arc^*}$ and other parameters were also examined (Peckley, 2007), but these did not yield correlations that are as strong as that shown in Fig. 24.

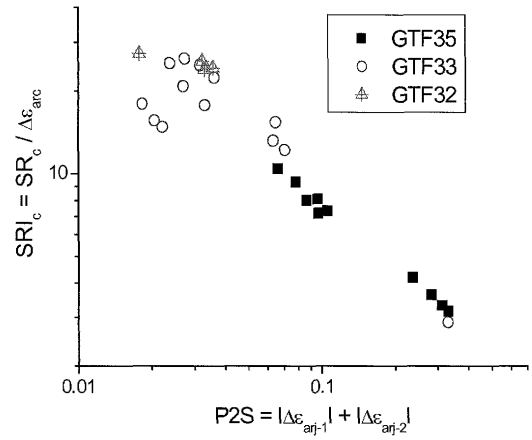

Fig. 25. SRI modulus vs. P2S of selected half-cycles 'c' and 'c*'

Again for brevity, the sum of the magnitudes of the increment in residual strain due to the preceding 2 half-cycles, is referred to from hereon as the preceding 2 half-cycle strains or, simply, P2S. When the quantity $SR_c/\Delta\varepsilon_{arc}$ or $SR_c\Delta\varepsilon_{arc^*}$ is plotted with P2S, as shown in Fig. 25, a fundamental behaviour in cyclic loading can be inferred. Note that the quantity $SR_c/\Delta\varepsilon_{arc}$ can be characterized as a modulus, referred to as SRI modulus in this study. When P2S is large, the corresponding SRI modulus becomes small and large increment in residual strain $\Delta\varepsilon_{arc}$ can be expected. The behaviour just described is one of the key findings in this study and is referred to here as "the P2S effect". Evidently, this effect has to be taken into account when estimating residual strains in soft rocks due to irregular cyclic loading.

The P2S Effect in Uniform Amplitude Cyclic Loading

Figures 26 and 27 present SR-CN and $\Delta\varepsilon_{ar}$-CN histories of selected loading stages from the tests conducted on samples designated as GTF30 and GTF31 (*see* also Peckley and Uchimura, 2007).

Figure 28, on the other hand, plots the data from all the cyclic loading stages applied on these samples, including GTF34, in terms of SRI and P2S.

It can be readily observed from Figs. 26 and 27 that the increment in residual strain due to positive half-cycles increases with loading cycle number. The same can be observed with the increments in residual strain due to negative half-cycles: the magnitude of these residual strain increments increases with cycle number. From Fig. 28, it is apparent that the P2S effect also plays an important role in softening behaviour under uniform amplitude cyclic loading. In fact, the figure appears to suggest that softening behaviour is a unique function of P2S such that a curve can be derived for positive half-cycles and another can be derived from negative half-cycles, as shown in the figure.

Quite a few remarks can be made from these observa-

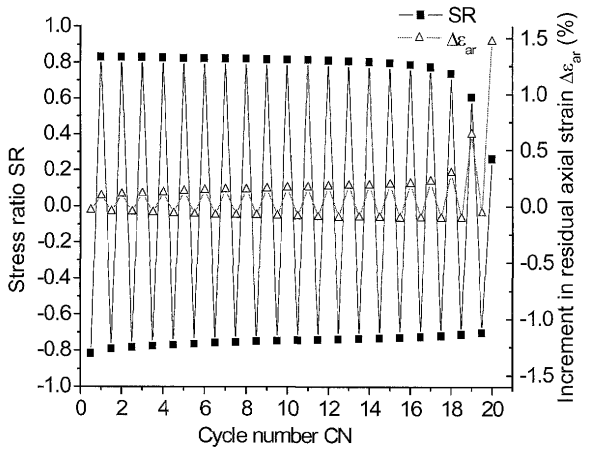

Fig. 26. GTF30 stress ratio SR & increment in residual strain-cycle number history: Stage S5

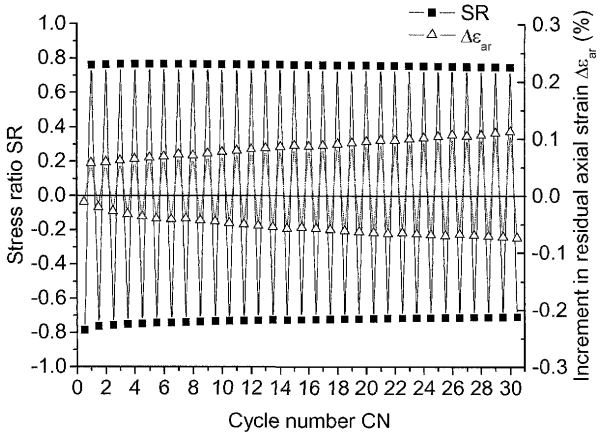

Fig. 27. GTF31 stress ratio SR & increment in residual strain-cycle number history: Stage S2

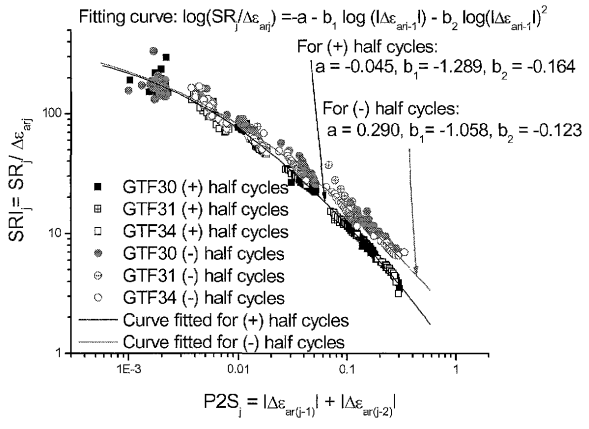

Fig. 28. SRI modulus vs. P2S from uniform cyclic loading tests

tions:

1) The increase in half-cycle residual strain increment with cycle number, as shown in Figs. 26 and 27, can be characterized as the result of cyclic loading degradation.
2) Such softening behaviour deviates from what is implied in fatigue model developed in *Faitgue Model* that there is a one-to-one correspondence between stress ratio and residual strain increment. Note that if these implied assumptions were true, there should be no change in residual strain increment no matter how many loading cycles are applied.
3) From the foregoing remarks, it can be inferred that by defining residual strain increment as the increment after a full cycle of loading (not as the increment due to a half-cycle), this softening behaviour was effectively hidden. In fact, the observation made in the *Fatigue Model* that residual strain accumulates linearly with increasing cycle number implies that no softening occurs with the number of loading cycles applied, which is contrary to what can be observed from Fig. 27.
4) In other words, when residual strain increment is defined as the increment due to a full cycle, a linear trend in residual strain accumulation with cycle number can still be observed even when softening occurs, because in one full cycle of loading, an increase in residual strain increment due to a positive half-cycle can be cancelled by an increase in the magnitude of the residual strain increment due to the negative half-cycle.
5) Evidently, softening behaviour can be better analyzed when residual strain increment and stress ratios are defined in terms of half-cycle loading.

From all the foregoing remarks and observations made in this section and previous sections, the reason for the large discrepancies between the measured residual strains and the results of simulations using the fatigue model derived in *Fatigue Model* is now apparent. The softening behaviour in irregular cyclic loading, in which P2S effect plays a prominent role, was not fully taken into account in the fatigue model. It can also be inferred that the P2S effect is an important factor to consider when quantifying cyclic loading degradation.

SIMULATIONS CONSIDERING THE P2S EFFECT

With the unique curves derived in Fig. 28, one for positive half cycles and the other for negative half cycles–simulations of the irregular cyclic loading tests on GTF32, GTF33 and GTF35 can be carried out. For brevity, such curves shall be referred to here as strain softening curves, or simply SS curves, and the particular set of SS curves shown in Fig. 28 is referred to as Model 1 SS curves. Since the first half cycle of loading cannot be simulated using only these strain softening curves, a relationship between the residual strain increment due to the first half cycle and the corresponding stress ratio was also derived. This relationship is shown in Fig. 29.

Figures 30 and 31 show the results of the simulations performed for GTF33 and GTF35 using the SS curves of Model 1 (Fig. 28) and the stress ratio-residual strain curves in Fig. 29. While it can be observed from Figs. 30(b) and 31(b) that the model seems to simulate the P2S

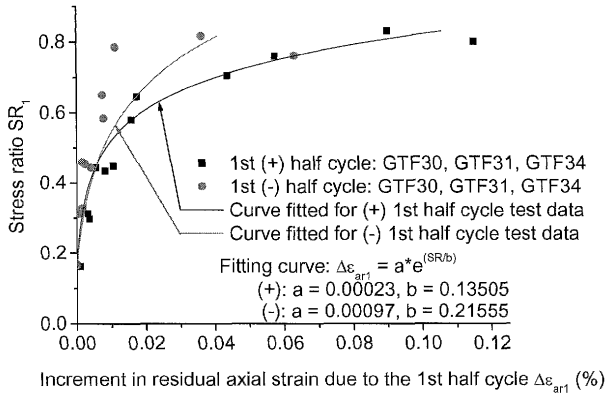

Fig. 29. Residual strain due to the 1st half cycle (GTF30, GTF31, GTF34)

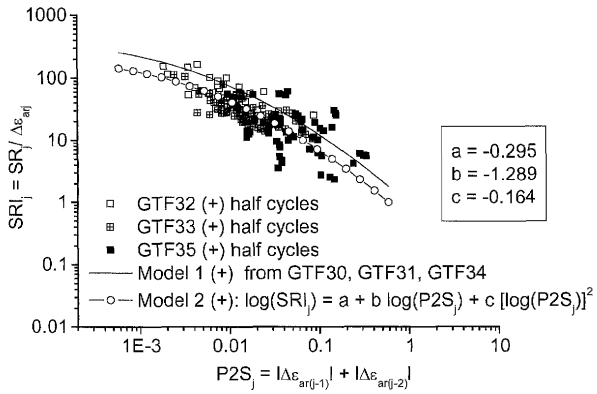

Fig. 32. Comparison between irregular cyclic loading data and softening Model 1 for (+) half cycles (*see* Fig. 28), Model 2 included

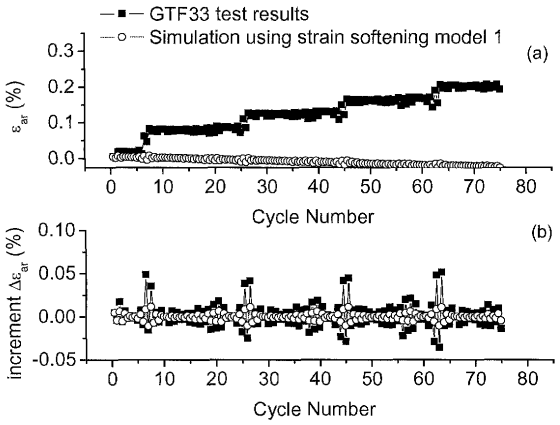

Fig. 30. Simulation of GTF33 test using strain softening Model 1 (*see* Fig. 28)

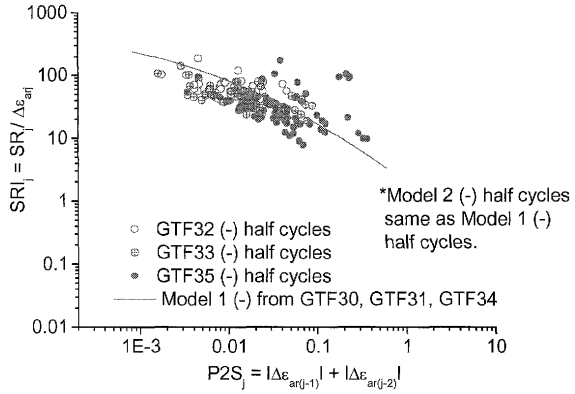

Fig. 33. Comparison between irregular cyclic loading data and softening Model 1 for (−) half cycles (*see* Fig. 28)

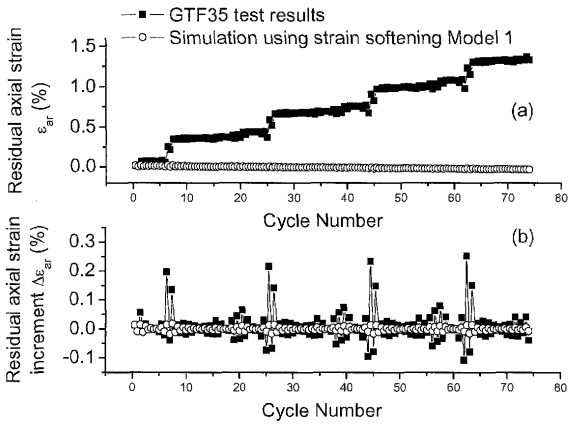

Fig. 31. Simulation of GTF35 test using strain softening Model 1 (*see* Fig. 28)

effect described in the previous chapter, overall the accumulation of residual strains was poorly simulated.

Figures 32 and 33 compare the irregular cyclic loading test data from GTF32, GTF33, and GTF35 with the SS curves of Model 1. Following are two reasons that could account for the large discrepancies between the test data and simulation results:

a) The SS curve of Model 1 for positive half cycles appears to be above most of the irregular cyclic loading tests data points.
b) The SS curves of Model 1 are too near each other. For larger residual strains to accumulate, the SS curves should be placed farther apart[4].

Considering the above conjectures on the discrepancies between simulation results and test data, the SS curve for positive half cycles in Model 1 was adjusted heuristically[5] to a position slightly lower than the perceived average of the irregular cyclic loading test data points, as shown in Fig. 32. The adjusted SS curve for positive half cycles and the SS curve for negative half cycles in Model 1 were renamed Model 2 SS curves. Note that no adjustment was made on the negative half-cycle SS curve.

Figures 34 and 35 show the simulation results using the

[4] As discussed in *The P2S Effect in Uniform Amplitude Cyclic Loading*, an SS curve represents a kind of a modulus that is dependent on the parameter P2S. In these simulations, the idea to estimate the residual strain given such an SS curve, the half-cycle loading amplitude and the P2S parameter, is explored. Note that the wider the divergence of between the positive half-cycle SS curve and the negative half-cycle SS curve, the larger is the residual strain obtained for one cycle of loading.

[5] Adjustments were carried out by trial and error taking into account the results of earlier simulations.

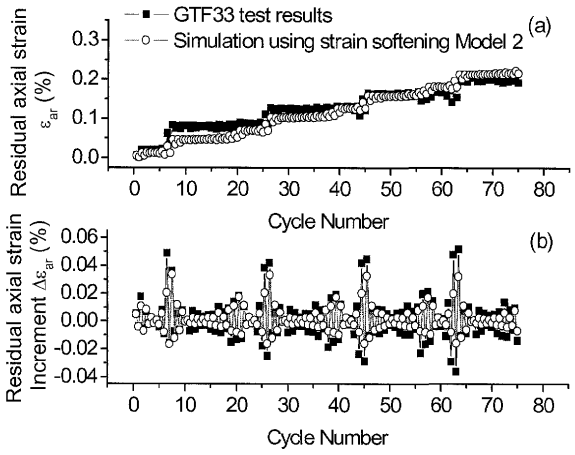

Fig. 34. Simulation of GTF33 test using strain softening Model 2 (*see* Figs. 32 and 33)

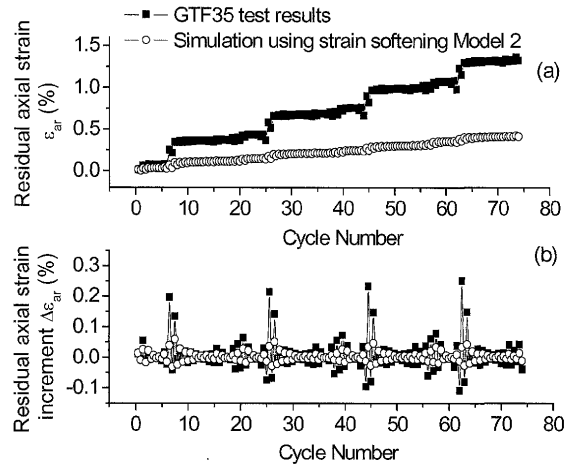

Fig. 35. Simulation of GTF35 test using strain softening Model 2 (*see* Figs. 31 and 32)

SS curves of Model 2. The following can be observed from these figures:

1) Unlike for the simulations using the SS curves of Model 1, the trend in the simulated accumulation of residual strain is consistent with the test data. The simulated residual strain generally increases with the number of cycles.
2) The accumulation of residual strains in GTF33 is reasonably replicated. That of GTF35, however, is largely underestimated.
3) The P2S effect is simulated in all samples, although the simulation results are not quantitatively accurate.

Given the conjectures from the first set of simulations and the observations made above-specifically observation (2) which can be attributed to the trend among the test data points that at higher P2S values, there is a wider divergence between the positive half cycle data points and negative half cycle data points, as shown in Fig. 36, the SS curves referred to as Model 3 were introduced[4,5,6].

[6] The main difference between Model 2 and Model 3 is that for Model 3, there is wider divergence between the SS curve for positive half-cycles and that for negative half-cycles is wider at higher values of P2S.

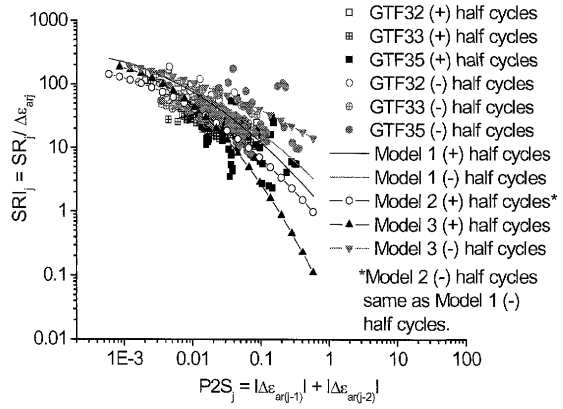

Fig. 36. Strain softening Model 3 together with test data and Models 1 and 2

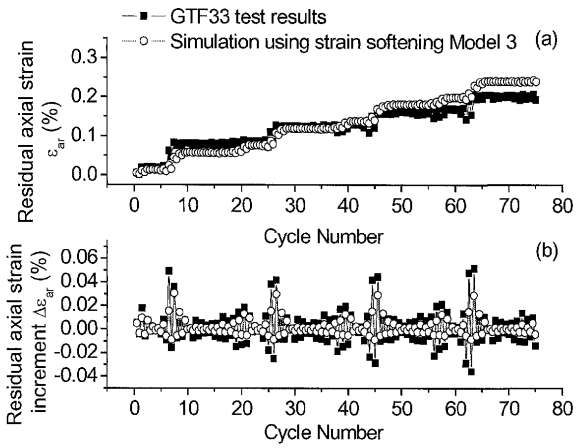

Fig. 37. Simulation of GTF33 test using strain softening Model 3 (*see* Fig. 36)

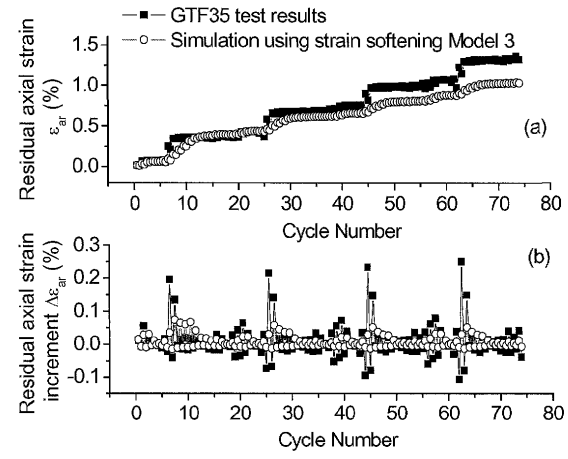

Fig. 38. Simulation of GTF35 test using strain softening Model 3 (*see* Fig. 36)

Figures 37 and 38 show the simulation results using Model 3. The following can be observed from these figures:

a) Similar to the case of Model 2, the trend in residual strain accumulation is consistent with the test data.

The residual strain generally increases with the number of cycles.

b) The accumulation of residual strains in GTF33 is also reasonably replicated. Compared with the simulation using Model 2, the accumulation of residual strain in GTF35 can also be said to be better simulated.

c) As in the case of Model 2, the P2S effect is simulated in all samples, but the simulation is not quantitatively accurate. It can be also inferred from these results and from Fig. 35 that different loading histories result in different SS curves.

Considering the significant scatter of irregular test data points in the SRI vs. P2S plot shown in Fig. 35, nonlinear curve fitting–involving the half cycle stress ratio SR_j, the corresponding increment in residual strain $\Delta\varepsilon_{arj}$, the quantity $P2S_j$ and the time elapsed for half cycle j referred to here as dt_j was carried out to derive other SS functions or curves. The simulation results from these SS functions were not necessarily any better than the procedure involved with Model 3 (Peckley, 2007).

CONCLUSIONS

Based on the results of tests and simulations that are presented in this paper, the following conclusions can be made:

(1) The use of fatigue modelling from uniform cyclic loading test data to simulate irregular cyclic loading can result in significant underestimation of residual strains. Residual strains are underestimated because fatigue modelling does not take into account the effect of the preceding two half-cycle residual strain increments on the softening behaviour of soft rocks, referred herein as P2S effect. The quantity P2S is defined as the sum of the magnitudes of the residual strain increments due to the preceding two half-cycles. When P2S is large, a large residual strain increment can be expected.

(2) From the simulation results presented in this paper, it is clear that taking the P2S effect into account can improve the simulation of residual strain accumulation due to irregular cyclic loading. Among these simulations, the simulations using SS curves from SRI vs. P2S plot in which the divergence between the SS curve for positive half-cycles and that of negative half-cycles becomes wider as the quantity P2S becomes larger, appear to yield results that are closest to the measured data. It should be noted, however, that the main drawback of this modelling procedure is that different loading histories result in different SS curves.

Considering the said drawback and all the simulation results presented in this study, it becomes apparent that soft rock testing programs should not be limited only to uniform cyclic loading tests. Irregular cyclic loading tests are as, if not more, important as uniform cyclic loading tests. Evidently, there is still much room for improving the modelling procedure that was explored in this paper. Aside from the P2S effect, another factor or other factors related to cyclic loading effects apparently still have to be identified and characterized.

ACKNOWLEDGMENTS

This research was made possible through a scholarship grant that was awarded to the first author by the Japan Ministry of Education, Culture, Sport, Science, and Technology (MEXT). The authors are also grateful for the assistance of Engr. Wilson A. Sy of Aromin & Sy+ Associates, Inc. in obtaining GTF soft rock samples from Fort Bonifacio, Metro Manila. Special appreciation is also extended to Prof. Junichi Koseki of the Koseki Laboratory of IIS, University of Tokyo and Prof. Fumio Tatsuoka of the Soil Mechanics Laboratory of the Tokyo University of Science for allowing the authors to use the sample preparation equipment and hydraulic testing apparatus of their laboratories.

REFERENCES

1) Allotey, N. and El Naggar, M. H. (2005): Cyclic soil degradation/hardening models: A critique, *Proc. 16th ICSMGE*, Osaka, Japan, 785–790.
2) ASTM (2000): D 5079-90 Standard practices for preserving and transporting rock core samples, *Annual Book of ASTM Standards*, **04.08** (Soil and Rock), 971–976.
3) Bautista, M. P. (2004): *Overview of the MMEIRS Project*, http://www.phivolcs.dost/clarification/Leyo's Letter.pdf.
4) Coviello, A., Lagioia, R. and Nova, R. (2005): On the measurement of the tensile strength of soft rocks, *Rock Mechanics and Rock Engineering*, **38**(4), 251–273.
5) Goto, S., Tatsuoka, F., Shibuya, S., Kim, Y. S. and Sato, T. (1991): A simple gauge for local small strain measurements in the laboratory, *Soils and Foundations*, **31**(1), 169–180.
6) Hayano, K., Matsumoto, M., Tatsuoka, F. and Koseki, J. (2001): Evaluation of time-dependent deformation properties of sedimentary soft rock and their constitutive modelling, *Soils and Foundations*, **41**(2), 21–38.
7) Indo, H. (2001): Cyclic triaxial tests on deformation properties of soft rocks, *Master of Engineering Thesis*, University of Tokyo (in Japanese).
8) Ishihara, K. and Yasuda, S. (1975): Undrained deformation and liquefaction of sand under cyclic stresses, *Soils and Foundations*, **15**(1), 45–59.
9) Kashima, N., Fukunaga, S., Saeki, M. and Koseki, J. (2000): Study on procedures to estimate earthquake-induced residual settlement of large scale bridge foundations (part 2), *Proc. 55th Annual Conference of Japan Society of Civil Engineers*, Section 1 (in Japanese).
10) Koseki, J., Moritani, T., Fukunaga, S., Tatsuoka, F. and Saeki, M. (2001): Analysis on seismic performance of foundation for Akashi Kaikyo Bridge, *Proc. 2nd Int. Symposium Pre-failure Deformation Characteristics of Geomaterials* (eds. by Jamiolowski et al.), Balkema, 1405–1412.
11) Nelson, A. R., Personius, S. F., Rimando, R. E., Punongbayan, R. S., Tungol, N., Hannah Mirabueno, H. and Rasdas, A. (2000): Multiple large earthquakes in the past 1500 years on a fault in Metropolitan Manila, The Philippines, *Bulletin of Seismological Society of America*, **90**, 73–85.
12) Originlab Corporation (2006): *Origin 7.5 SR6 On-line Manual*.
13) Peckley, D. C. (2007): Strength and deformation of soft rocks under cyclic loading–an empirical study focusing on residual strain accumulation and loading period effects, *PhD Dissertation*, University of Tokyo.
14) Peckley, D. C. and Uchimura, T. (2006): Strength and deformation

characteristics of soft rocks from the Guadalupe Tuff Formation in Metro Manila when subjected to large cyclic loading, *Proc. 3rd International Conference on Urban Earthquake Engineering*, Tokyo Institute of Technology, Japan, 137–144.

15) Peckley, D. C. and Uchimura, T. (2007): Strength and deformation of soft rocks under cyclic loading considering loading period effects, *Soils and Foundations*, **49**(1), 51–62.
16) Salas Monge, R. (2002): Effects of large amplitude cyclic loading on deformation and strength properties of cement treated sand, *Master of Engineering Thesis*, University of Tokyo.
17) Seed, H. B. and Idriss, I. M. (1971): A simplified procedure for evaluating soil liquefaction potential, *Journal of SMFE Div.*, ASCE, **97**(9), 249–274.
18) Seed, H. B., Idriss, I. M., Makdisi, F. and Banerjee, N. (1975): Representation of irregular stress time histories by equivalent uniform stress series in liquefaction analysis, *Report No. EERC 7529*, Univ. of California, EERC, Berkeley.
19) Tatsuoka, F. and Silver, M. (1981): Undrained stress-strain behaviour of sand under irregular loading, *Soils and Foundation*, **21**(1), 51–66.
20) Tatsuoka, F., Maeda S., Ochi, K. and Fujii, S. (1986): Prediction of cyclic undrained strength of sand subjected to irregular loadings, *Soils and Foundations*, **26**(2), 73–90.
21) Tatsuoka, F., Hayano, K. and Koseki, J. (2003): Strength and deformation characteristics of sedimentary soft rocks in the Tokyo Metropolitan Area, *Characterization and Engineering Properties of Natural Soils* (eds. by Tan et al.), Swets and Zeitlinger, 1461–1525.
22) Yamagata, M., Yasuda, M., Nitta, A. and Yamamoto, S. (1996): Effects on the Akashi Kaikyo Bridge, *Special Issue of Soils and Foundations on Geotechnical Aspects of the January 17, 1995 Hyogoken-Nambu Earthquake*, 179–187.